

Multi-target quantum compilation algorithm

Vu Tuan Hai^{1,*}, Nguyen Tan Viet², Jesus Urbaneja³, Nguyen Vu Linh^{4,5}, Lan Nguyen Tran^{4,5†}, and Le Bin Ho^{6,7‡}

¹Nara Institute of Science and Technology, Ikoma 630-0192, Nara, Japan

²FPT University, Hanoi, Vietnam

³Department of Mechanical and Aerospace Engineering, Tohoku University, Sendai 980-0845, Japan

⁴University of Science, Vietnam National University, Ho Chi Minh City 70000, Vietnam

⁵Vietnam National University, Ho Chi Minh City 70000, Vietnam

⁶Frontier Research Institute for Interdisciplinary Sciences, Tohoku University, Sendai 980-8578, Japan

⁷Department of Applied Physics, Graduate School of Engineering, Tohoku University, Sendai 980-8579, Japan

*vu.tuan.hai.vr7@naist.ac.jp

†lantrann@gmail.com

‡binho@fris.tohoku.ac.jp

ABSTRACT

In quantum computing, quantum compilation involves transforming information from a target unitary into a trainable unitary represented by a quantum circuit. Traditional quantum compilation optimizes circuits for a single target. However, many quantum systems require simultaneous optimization of multiple targets, such as simulating systems with varying parameters and preparing multi-component quantum states. To address this, we develop a multi-target quantum compilation algorithm to enhance the performance and flexibility of simulating multiple quantum systems. Through our benchmarks and case studies, we demonstrate the algorithm's effectiveness, highlighting the significance of multi-target optimization in the advancement of quantum computing. This work establishes the groundwork for further development, implementation, and evaluation of multi-target quantum compilation algorithms.

1 Introduction

Variational quantum algorithms (VQAs) like quantum approximate optimization algorithm (QAOA), variational quantum eigensolver (VQE), quantum neural networks (QNN), and quantum compilation (QC) are promising for solving practical tasks on noisy intermediate scale quantum (NISQ) devices beyond classical computers¹. Recent achievements demonstrate effectiveness in quantum state preparation^{2–6}, quantum dynamic simulation^{2,7–9}, and quantum metrology^{10–14}. QC, in particular, has gained significant interest. It uses a training process to transform information from an unknown target unitary into a trainable known unitary^{15,16}. This method has various applications, including gate optimization¹⁵, quantum-assisted compiling¹⁶, continuous-variable quantum learning¹⁷, quantum state tomography¹⁸, and quantum objects simulation². For instance, a quantum object such as a quantum state can be prepared and its evolution can be simulated in a quantum circuit by using QC².

The performance of QCs relies on the number of qubits and the circuit depth. The choice of

ansatzes (trainable quantum circuits) is also crucial and must be carefully selected. Some entangled topologies have shown promise in solving quantum state preparation problems but require many resources due to their numerous layers and parameters⁶. Traditional QC focus on compiling a single target, like the topography of a single quantum state¹⁸ or the preparation of a single quantum object (e.g., a quantum state, Hamiltonian)². However, many scenarios require multiple targets, such as simulating systems with varying parameters, preparing multi-component quantum states, tomography for multiple states, and optimizing algorithms for different instances. Therefore, it is crucial to develop an effective automatic approach for these tasks.

This work presents a multi-target quantum compilation algorithm to address the need to handle multiple targets. We compile multiple unitaries into a single trainable unitary through an optimization process, improving QC performance and applicability in practical scenarios. We explain the theoretical foundations of our algorithm, its structure, and using techniques like the genetic algorithm (GA) to enhance the multi-target QC process. We show the effectiveness of our algorithm through benchmarking and case studies, including the preparation of thermal states and the simulation of time-dependent Hamiltonians. The results highlight the importance of multi-target compilation in advancing quantum computing technologies and the potential for further innovation in this field.

2 Results

2.1 Multi-target quantum compilation

Quantum compilation (QC)^{6,16} is a training process that transforms information from a target unitary U to a trainable unitary $V(\boldsymbol{\theta})$, where $\boldsymbol{\theta}$ are trainable parameters. Hereafter, we introduce a compilation process to transform a set of n targets into one trainable unitary, therefore, it is called multi-target quantum compilation.

Definition

Let \mathcal{H} be a Hilbert space, and $\mathcal{U} = \{U_j; 1 \leq j \leq n\}$ be n -target unitaries on \mathcal{H} , there exists a trainable unitary V that satisfies

$$U_j V^\dagger(\boldsymbol{\theta}_j) = e^{-i\phi} \mathbb{I}, \quad \forall 1 \leq j \leq n, \quad (1)$$

where $\boldsymbol{\theta}_j \in \{\theta_j^{(1)}, \theta_j^{(2)}, \dots, \theta_j^{(m)}\}$ is a set of m trainable parameters and ϕ is a global phase. For each U_j , we need to maximize the kernel $\mathcal{K}_{U_j, V}(\boldsymbol{\theta}_j) = |\langle \psi | U_j V^\dagger(\boldsymbol{\theta}_j) | \psi \rangle|^2$ where $|\psi\rangle$ is a reference state. For maximizing all $\mathcal{K}_{U_j, V}(\boldsymbol{\theta}_j)$, $\forall U_j \in \mathcal{U}$, we define a cost function \mathcal{L} , which is the average infidelity

$$\mathcal{L}(\boldsymbol{\Theta}) = 1 - \frac{1}{n} \sum_{j=1}^n \mathcal{K}_{U_j, V}(\boldsymbol{\theta}_j), \quad (2)$$

where $\boldsymbol{\Theta} = (\boldsymbol{\theta}_1, \dots, \boldsymbol{\theta}_n)$ are trainable parameters, and $0 \leq \mathcal{L}(\boldsymbol{\Theta}) \leq 1$. The optimization process is to find $\boldsymbol{\Theta}^* = \text{argmin}_{\{\boldsymbol{\Theta}\}} \mathcal{L}(\boldsymbol{\Theta})$.

Quantum compilation algorithm

The training process in QC is a variational quantum algorithm (VQA). Given a target unitary U , it employs a gradient-based optimizer to update an ansatz $V(\boldsymbol{\theta})$ and find the optimal $\boldsymbol{\theta}^*$. The ansatz V is usually a multi-layer structure

$$V(\boldsymbol{\theta}) = \prod_{k=1}^L G_k(\boldsymbol{\theta}_k) \in \mathrm{SU}(2^N), \quad (3)$$

where $G_k(\boldsymbol{\theta}_k)$ is a sequence of parameterized single- and multi-qubit quantum gates, L is the number of layers, N the number of qubits. The design of $V(\boldsymbol{\theta})$ is not unique, and recent efforts to optimize it, including architecture search^{19–22}, adaptive variational quantum algorithm^{7,23}, and genetic-based approach (GA)^{24–27}.

In this work, we combine GA with VQA to optimize multi-target quantum compilation. This approach optimizes both the parameters and the structure of quantum circuits, ensuring efficient compilation, practical computational capability, and low-depth circuits. The scheme is shown in Fig.1a, and the flow chart is in Fig.1b. The genetic search identifies the best ansatz V^* that meets all inputs at a given threshold. The best ansatz is then used in VQA to find the optimal parameters $\boldsymbol{\Theta}^*$ using gradient descent.

Denote the set of generated quantum circuits as $\mathcal{V} = \{V_l; 1 \leq l \leq n_{\mathcal{V}}\}$, where $n_{\mathcal{V}}$ is the number of circuits. Each circuit $V_l \in \mathcal{V}$ is created from a pool of quantum gates. For each circuit V_l , we evaluate the average infidelity using

$$\mathcal{L}(\boldsymbol{\Theta}, V_l) = 1 - \frac{1}{n} \sum_{j=1}^n \mathcal{K}_{U_j, V_l}(\boldsymbol{\theta}_j), \quad \forall 1 \leq l \leq n_{\mathcal{V}}. \quad (4)$$

Following the flowchart, if $\mathcal{L}(\boldsymbol{\Theta}, V_l) \leq \text{threshold}$, we designate V_l to the best circuit, $V^* \leftarrow V_l$, and $\boldsymbol{\Theta}$ will be the optimal parameters, $\boldsymbol{\Theta}^* \leftarrow \boldsymbol{\Theta}$. If not, we run the VQA scheme with gradient descent to update $\boldsymbol{\Theta}$ for a certain number of iterations n_{iter} . Then, we use GA with selection, crossover, and mutation to create the next generation of \mathcal{V} . See the Method for a detailed evolution of the GA. The GA scheme repeats until the threshold is met or the number of generations n_{gene} is reached. Finally, if n_{gene} is reached without meeting the threshold, we pass the best circuit V^* to the VQA scheme again, and optimize $\boldsymbol{\Theta}$ until the threshold is met.

In this framework, we run the VQA process twice. The first run aims to create a suitable $\mathcal{L}(\boldsymbol{\Theta}, V_l)$ for evaluating the GA evolution process. We can choose a small n_{iter} in this step to reduce computational cost. The second run occurs after the GA and aims to optimize $\boldsymbol{\Theta}$ to ensure that $\mathcal{L}(\boldsymbol{\Theta}^*, V^*)$ is minimized within the best circuit V^* .

Our scheme differs from the one-stage¹⁹ and two-stage architecture search^{21,28}. In those methods, all circuits are generated, their cost functions are evaluated, and they are sorted from best to worst to select the top one. In our approach, each circuit $V_l \in \mathcal{V}$ is evaluated and compared with the best circuit (initially set as V_1). We thus do not require space to store all circuits. Although genetic algorithms have been suggested for quantum state tomography²⁹, we believe they are also promising for different types of VQAs, including our proposed method for quantum compilation.

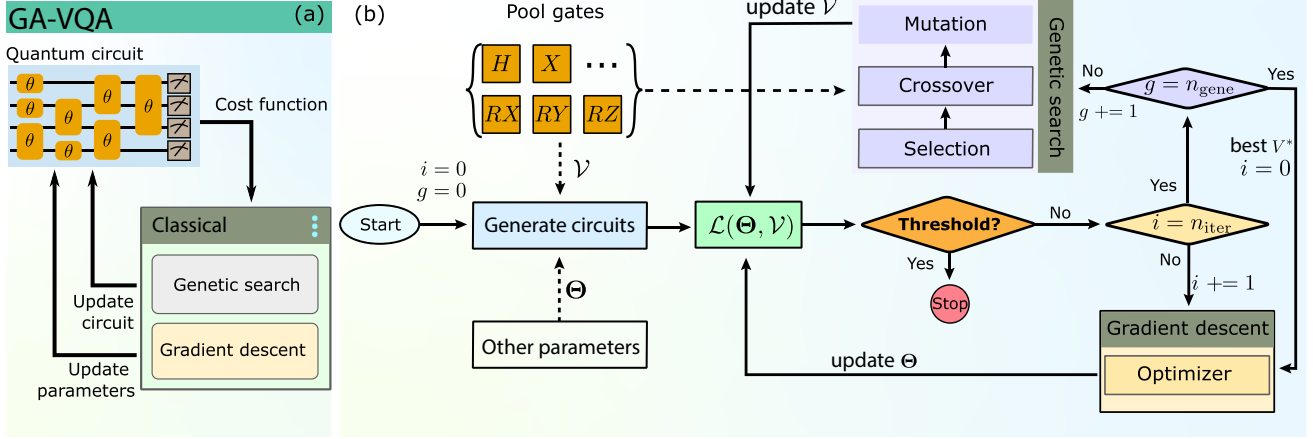


Figure 1. Integrated Genetic Approach with Variational Quantum Algorithm (GA-VQA) for multi-target quantum compilation optimization.

(a) The GA-VQA scheme involves a parameterized quantum circuit and a classical computer to evaluate and update the circuit and its parameters. (b) The flowchart: (i) Generate a set of circuits \mathcal{V} and parameters Θ , (ii) Evaluate the cost function $\mathcal{L}(\Theta, V_l)$ for all l . (iii) If it fails to pass, run VQA followed by GA to find the best circuit, checking the threshold each time. (iv) If the threshold is not met, pass the best circuit V^* to VQA and repeat until the threshold is met.

Numerical illustration

For numerical evaluation, we follow Ref.³⁰ and divide a random set \mathcal{U} into a training set $\mathcal{U}_{\text{train}} = \{U_1, U_2, \dots, U_{\text{train}}\}$ and a testing set $\mathcal{U}_{\text{test}} = \{U_{\text{train}+1}, U_{\text{train}+2}, \dots, U_n\}$. We then train the model on $\mathcal{U}_{\text{train}}$ using the cost function \mathcal{L} , where

$$\mathcal{L}(\Theta_{\text{train}}, V_l) = 1 - \frac{1}{n_{\text{train}}} \sum_{j=1}^{n_{\text{train}}} \mathcal{K}_{U_j, V_l}(\theta_j), \quad (5)$$

After training, we get the best circuit V^* and evaluate the expected risk \mathcal{R}

$$\mathcal{R}(\Theta_{\text{test}}) = \frac{1}{4} \mathbb{E}_{U_j \in \mathcal{U}_{\text{test}}} \left\| U_j |\mathbf{0}\rangle\langle \mathbf{0}| U_j^\dagger - [V^*]^\dagger(\theta_j) |\mathbf{0}\rangle\langle \mathbf{0}| V^*(\theta_j) \right\|_1^2. \quad (6)$$

Note that we fixed $|\psi\rangle = |\mathbf{0}\rangle \equiv |0\rangle^{\otimes N}$.

Figure 2(a-d) shows the correlation between risk \mathcal{R} and fidelity $\mathcal{F} = 1 - \mathcal{L}$ for several n_{gene} and $n_{\mathcal{V}}$ with $N = 3$. The GA-VQA method identifies a low-risk, high-fidelity ansatz for multi-target Haar random unitaries. Additionally, the factors n_{gene} and $n_{\mathcal{V}}$ have minimal impact on the results, allowing GA-VQA to run efficiently with minimal values, thus saving computational resources. Figure 2e shows fidelity versus depth d for 2-5 qubits. As expected, higher N requires larger d to achieve high fidelity. In the figure, circles mark the depth where $\mathcal{F} \geq 0.99$, with upper bounds generated by the standard Qiskit method. Figure 2f shows the best circuit generated by our GA-VQA compared to the Qiskit-generated circuit in Fig. 2g and the $|g_2 g_N\rangle$ ansatz⁶ in Fig. 2h for $N = 3$. The GA-VQA circuit has the smallest depth. Table 1 shows detailed comparisons for 2 to

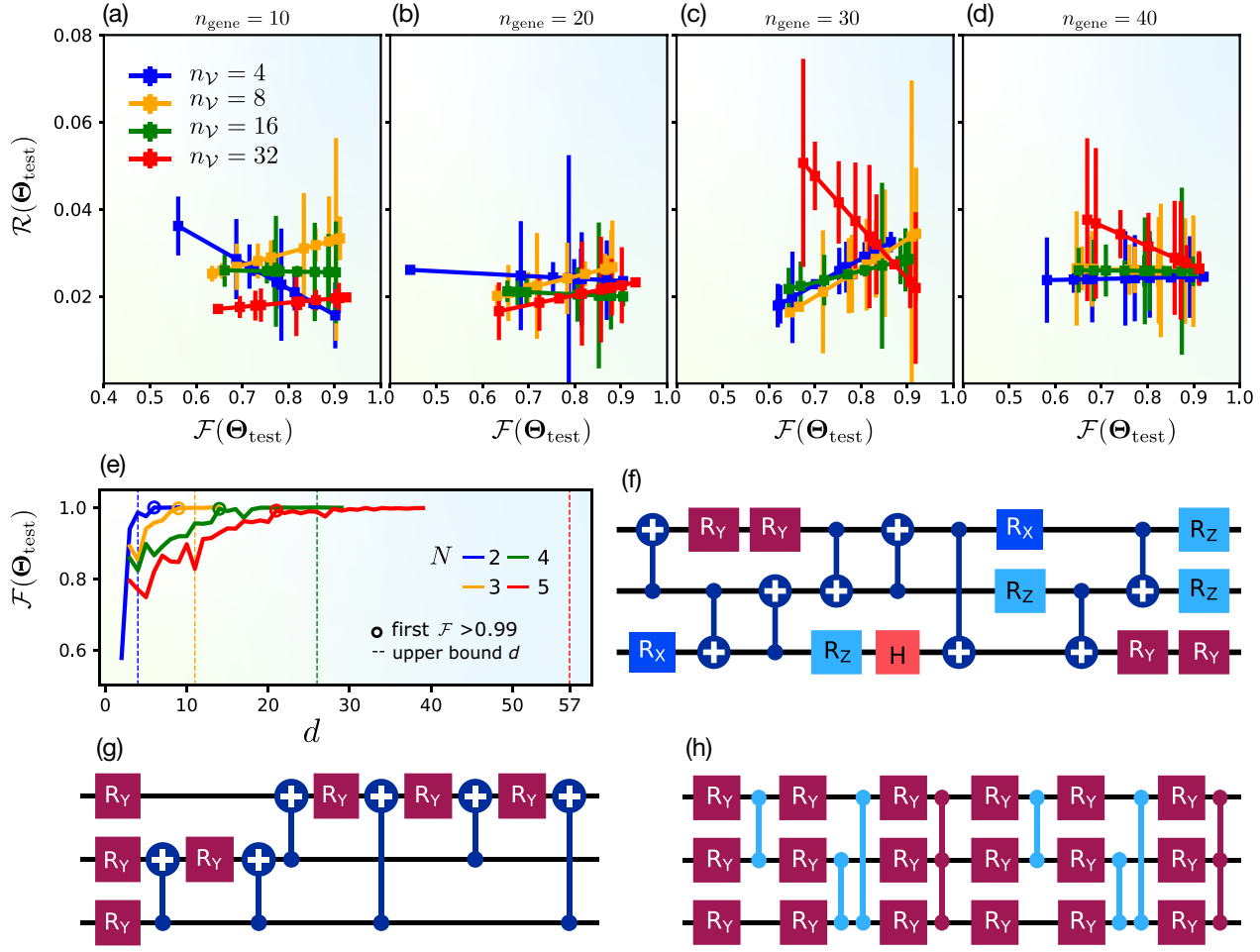


Figure 2. Numerical benchmarking for a set of Haar random \mathcal{U} . (a-d) Correlation between risk and fidelity for different number of generations n_{gene} and circuits per generation n_V . (e) Plot of fidelity versus depth d for different number of qubits N ranging from 2 to 5. (f) The best quantum circuit generated by GA-VQA. (g) The quantum circuit generated by Qiskit. (h) $|g2g_N\rangle$ (2 layers) ansatz before transforming into single and two-qubit gates.

5 qubits, demonstrating that the GA-VQA circuit provides the highest fidelity with the smallest depth.

2.2 Applications

Thermal state preparation (TSP)

Quantum state preparation using quantum algorithms is well-studied for pure states^{3,5,6}. However, preparing mixed states requires purification first and then preparing the pure state³¹. The conventional purification method needs $2N$ qubits to prepare a mixed state of N qubits. Here, we propose a “dense-purification” method that needs only N qubits.

A quantum state ρ in an n -dimensional Hilbert space \mathcal{H}_A can be represented using its eigenvalues and eigenstates as $\rho = \sum_{j=1}^n p_j |j\rangle\langle j|$. In conventional purification, we create a pure state $|\psi\rangle$ in a larger Hilbert space $\mathcal{H}_A \otimes \mathcal{H}_B$, where \mathcal{H}_B is another n -dimensional Hilbert space with an orthonormal

Table 1. Comparison between three methods: GA-VQA, default Qiskit preparation, and $|g_2g_N\rangle$ (2 layers). All circuits are transpiled with the same gate set $\{H, S, CX, R_i(\theta)\}$ with $i \in \{x, y, z\}$.

N	\mathcal{F}			Depth (d)			#gates (#1-qubit gate + #2-qubits gate)			#parameters		
				GA-VQA	Qiskit	$ g_2g_N\rangle$	GA-VQA	Qiskit	$ g_2g_N\rangle$	GA-VQA*	Qiskit	$ g_2g_N\rangle$
2	0.92	0.99	0.99	3	4	24	4+1	3+2	24+6	5	3	12
3	0.99	0.99	0.99	9	11	38	17+5	7+6	40+18	17	7	18
4	0.99	0.99	0.99	15	26	97	32+14	15+14	104+52	40	15	24
5	0.99	0.99	0.97	27	57	166	63+36	31+30	158+98	73	31	30

*The number of parameters in GA-VQA differ for each run depending on the set of gates in the best circuit.

basis $\{|j\rangle_B\}$. The pure state is $|\psi\rangle = \sum_j \sqrt{p_j} |j\rangle_A |j\rangle_B$, purifying ρ such that $\rho = \text{Tr}_B[|\psi\rangle\langle\psi|]$. In our dense-purification method, we define a pure state $|\psi\rangle = \sum_j \sqrt{p_j} |j\rangle$, directly representing the dense-purified state of ρ . It can be shown that $\rho = \text{diag}(|\psi\rangle\langle\psi|)$, allowing us to extract various properties of ρ from $|\psi\rangle$.

We demonstrate the preparation of thermal equilibrium states, specifically Gibbs states at fixed temperatures. These states are crucial for various applications, such as quantum simulation³², quantum machine learning³³, quantum condensed matter³⁴, quantum field theory³⁵, and cosmology^{36,37}. We focus on the Gibbs state of a transverse field Ising model (TFIM)³⁸, which is useful for studying thermal phase transitions in condensed matter physics.

In the TFIM model on a ring of N sites, the Hamiltonian takes the form $H = \sum_{i=1}^N Z_i Z_{i+1} + \sum_{i=1}^N X_i$, where X and Z are Pauli matrices. In this model, the Gibbs state is defined as $\rho(\beta) = e^{-\beta H}/Z(\beta)$ where $\beta = k_B T$ is the inverse temperature and $Z(\beta) = \text{Tr}[e^{-\beta H}]$ is the partition function. At $\beta = 0$, the Gibbs state is maximally mixed, and it gradually becomes a pure state when $\beta \rightarrow \infty$.

Conventionally, to prepare this mixed state on a quantum computer, previous approaches used the conventional purification scheme as^{4,39–41}

$$|\psi(\beta)\rangle = \frac{1}{\sqrt{Z(\beta)}} \sum_j e^{-\beta E_j/2} |j\rangle_A |j\rangle_B, \quad (7)$$

where $Z(\beta) = \sum_j e^{-\beta E_j}$. Here, E_j and $|j\rangle$ are the eigenvalues and eigenstates of H , i.e., $H|j\rangle = E_j|j\rangle$. The purified state is known as thermofield double (TFD) state⁴, which is related to the Gibbs state through $\rho(\beta) = \text{Tr}_B[|\psi(\beta)\rangle\langle\psi(\beta)|]$.

For the dense-purification approach, the dense-purified state is given by

$$|\psi_{\text{dense}}(\beta)\rangle = \frac{1}{\sqrt{Z(\beta)}} \sum_j e^{-\beta E_j/2} |j\rangle_A. \quad (8)$$

Previously, QAOA^{4,39,40,42} and parametrized circuits⁴¹ were used to prepare the quantum state in (7). Here, we apply our GA-VQA to prepare the states in Eqs.(7, 8). We evaluate the closeness of the prepared state to the target state using fidelity and purity metrics

$$\mathcal{F} = \text{Tr} \left[\sqrt{\sqrt{\rho(\beta)} \tilde{\rho}(\beta) \sqrt{\rho(\beta)}} \right]^2; \quad \text{and} \quad \mathcal{P} = \text{Tr}[\tilde{\rho}(\beta)], \quad (9)$$

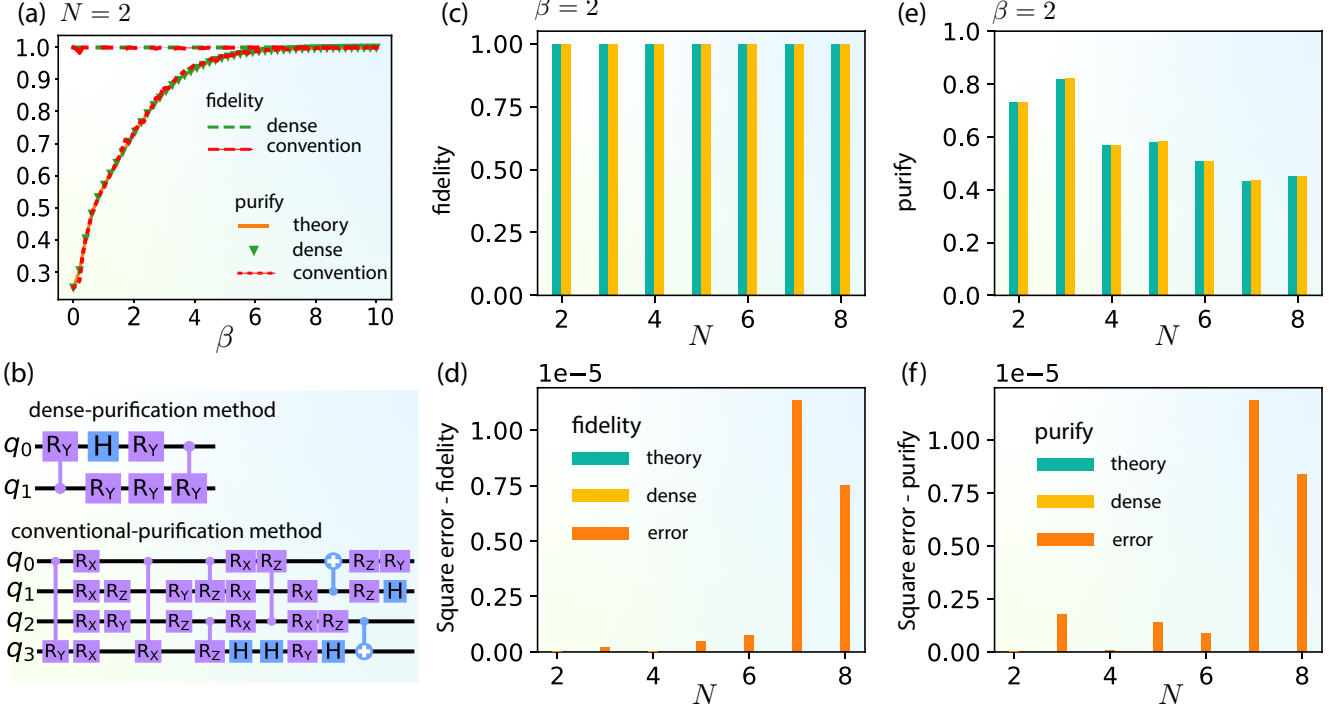


Figure 3. Thermal states preparation. (a) Comparison of fidelity and purity versus β at $N = 2$ for various methods, alongside theoretical predictions. (b) Quantum circuits used in dense and conventional methods. (c) Fidelity plotted against N at $\beta = 2$. (d) Square error of fidelity plotted against N at $\beta = 2$. (e) Purity plotted against N at $\beta = 2$. (f) Square error of purity plotted against N at $\beta = 2$.

where $\check{\rho}(\beta) = \text{Tr}[\lvert\psi(\beta)\rangle\langle\psi(\beta)\rvert]$ for conventional purification and $\check{\rho}(\beta) = \text{diag}[\lvert\psi_{\text{dense}}(\beta)\rangle\langle\psi_{\text{dense}}(\beta)\rvert]$ for dense purification. See the Method section for details on preparing $\lvert\psi(\beta)\rangle$ and $\lvert\psi_{\text{dense}}(\beta)\rangle$.

In Fig. 3a, we set $N = 2$ and examine \mathcal{F} and \mathcal{P} while comparing them in different methods. We demonstrate that both methods align well with the theory, proving the efficacy of the preparation method for creating Gibbs states. In Fig. 3b, we show the corresponding quantum circuits, where the dense method requires fewer qubits and lower circuit depth compared to the conventional method. Next, we focus on the dense method with $\beta = 2$. Figure 3c shows the fidelity versus the number of qubits N with the results closely approaching one (theory) for all N , and the square error is on the order of 10^{-5} as depicted in Fig. 3d. Similarly, we analyze the purity and its error in Fig. 3(e,f), which align well with the theory.

Time-dependent quantum dynamic simulation (TD-QDS)

In this section, we demonstrate for dynamic time-dependent simulations. We consider a one-dimensional spin-1/2 system with N spins, initially prepared in a domain wall configuration $\lvert\psi_0\rangle = \lvert\cdots\downarrow\downarrow\uparrow\uparrow\cdots\rangle$. The time-dependent Hamiltonian is given by

$$H(t) = -\frac{J}{2} \sum_{j=1}^{N-1} \left[\left(1 - \frac{t}{T}\right) X_j X_{j+1} + \left(1 + \frac{t}{T}\right) Y_j Y_{j+1} \right] + u \sum_{j=1}^{N-1} Z_j Z_{j+1} + h \sum_{j=1}^N X_j, \quad (10)$$

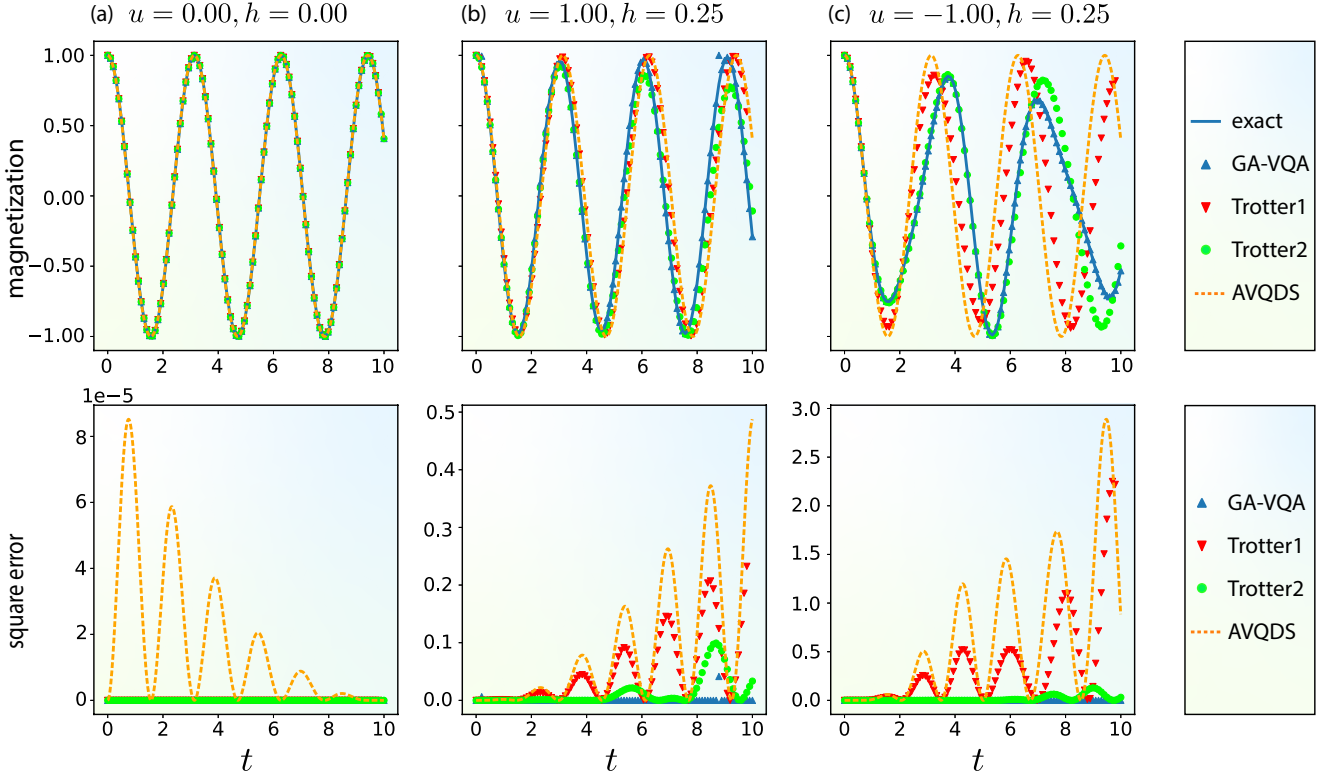


Figure 4. Time-dependent quantum dynamic simulation. Plot of the local magnetization versus time (upper) and its square error (lower) for several models: (a) $u = 0.00, h = 0.00$, (b) $u = 1.00, h = 0.25$, (c) $u = -1.00, h = 0.25$. Here we set $N = 2$, $J = 1$ and $T = 10$. We compare various methods with the theory, including GA-VQA, Trotter1, Trotter2, and AVQDS.

where J and u are coupling strengths, h is the external magnetic field, and X, Y, Z are Pauli matrices. The evolution is given by

$$U(t) = \mathcal{T} \exp \left(-i \int_0^t ds H(s) \right), \quad (11)$$

where \mathcal{T} is the time-ordering operator, and $\hbar = 1$ is used throughout the paper. We consider the local magnetization as the dynamical quantity to be examined

$$M_j(t) = \langle \psi(t) | Z_j | \psi(t) \rangle, \quad (12)$$

where $|\psi(t)\rangle$ is the quantum state given at time t .

The local magnetization is shown in Fig. 4, comparing the exact result with various methods, including GA-VQA, Trotterization^{43,44} with first order (Trotter1) and second order (Trotter2), and Adaptive Variational Quantum Dynamics Simulations (AVQDS)⁷. We set $N = 2$, $J = 1$, $T = 10$ and consider several models for u and h as shown in the figure. For the theoretical computation, the local magnetization is given by Eq. (12), with the final state directly computed from $U(t)$ yielding $|\psi(t)\rangle = U(t)|\psi_0\rangle$. For the other simulation methods, the local magnetization is derived from the measured probabilities of the final circuit. See detailed calculation in the Method section.

The GA-VQA results closely match the exact results over time for all models, demonstrating the method’s reliability and versatility in capturing quantum dynamics. Trotter2 also achieves high accuracy, aligning well with exact results in cases (a) and (b), but shows deviations in case (c). Trotter1 and AVQDS match well with theoretical predictions only in case (a) and deviate as time t increases in cases (b) and (c). Deviations in Trotter1 are common, as noted in previous studies^{43–45}, while discrepancies in AVQDS results stem from simplifications in our calculations, as discussed in the Method section.

3 Discussion

3.1 Demo application for Variational Quantum Eigensolver (VQE)

In this section, we extend the proposed multil-target compilation approach into VQE. It is a quantum algorithm used to estimate the lowest eigenvalue of a given Hamiltonian, which is crucial in quantum chemistry and optimization problems. It employs a parameterized quantum circuit to prepare trial states and a classical optimization routine to adjust these parameters iteratively, converging towards the lowest eigenvalue. This algorithm is handy in problems where the direct calculation of eigenvalues is computationally expensive, making it a promising candidate for near-term quantum computer applications.

The unitary coupled cluster with singles and doubles (UCCSD) ansatz was used in the first proposal of the VQE algorithm⁴⁶. While achieving high accuracy and attracting significant research interest, the UCCSD ansatz requires a large number of gates and a high depth⁴⁷, due to their “staircase” structure. This makes it less suitable for the Noisy Intermediate-Scale Quantum (NISQ) era.

Here, we apply the developed GA-VQA to find a more efficient ansatz for electronic structure ansatz. For this purpose, we use the cost function as the energy

$$\mathcal{L}_{\text{VQE}}(\Theta, V_l) = \sum_{j=1}^n \langle \mathbf{0} | V_l^\dagger(\boldsymbol{\theta}_j) H_j V_l(\boldsymbol{\theta}_j) | \mathbf{0} \rangle ; \forall 1 \leq l \leq n_V. \quad (13)$$

where $|\mathbf{0}\rangle \equiv |0\rangle^{\otimes N}$ is a reference state, $H_j \in \mathcal{H} \forall j = \{1, \dots, n\}$ is a set of n Hamiltonians with respect to the molecular distances $R = \{R_1, R_2, \dots, R_n\}$, and V_l is a quantum circuit found by GA-VQA scheme.

We apply the GA-VQA scheme to the Hydrogen molecule. In Fig. 5a, we estimate the ground state potential energy surface by optimizing VQE with the best ansatz from the GA-VQA method for ten points ($n = 10$), achieving accuracy comparable to the UCCSD ansatz. Here, we approximate the UCCSD ansatz with only the first-order Suzuki-Trotter approximation. Figure 5b shows the convergence of fidelity versus n_{gene} for $d = 15, 18, 20, 24$, and 25 , with their best fidelities plotted in Fig. 5c. As seen in Fig. 5d, the ansatzes identified by GA-VQA possess more parameters compared to UCCSD ansatz but require significantly less depth. Even with the first-order Trotter decomposition, the UCCSD ansatz demands a depth of 74. Consequently, the GA-VQA found ansatzes are more suitable for the NISQ era.

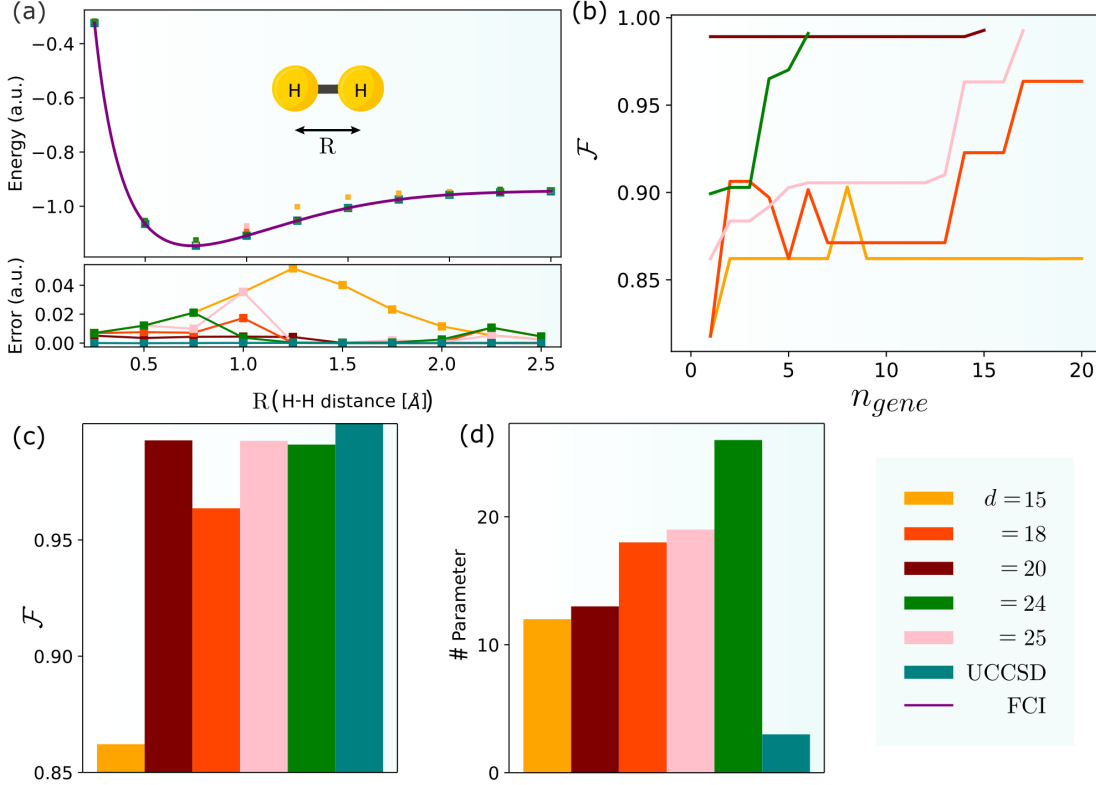


Figure 5. The application of GA-VQA scheme to Variational Quantum Eigensolver Algorithm for Hydrogen molecule (a) Comparison of UCCSD ansatz and GA-VQA found ansatz in estimating ground state energy surface of the Hydrogen molecule. (b) The fidelity for different depth GA-VQA found ansatz as a function of optimization step n_{gene} . (c) The best fidelity of GA-VQA found and UCCSD ansatz. (d) The number of parameters in GA-VQA found and UCCSD ansatz.

3.2 The complexity of GA-VQA

We discuss here the complexity of GA-VQA. The time complexity of GA-VQA is defined as $\mathcal{O}(n_{\text{gene}}n_{\mathcal{V}}\mathcal{F})$ which depends on the number of generations n_{gene} , the number of circuits in each generation $n_{\mathcal{V}}$ and the complexity of the fitness function \mathcal{F} . When the fitness of circuits in one generation can be evaluated concurrent, the actual time complexity is $\mathcal{O}(\frac{n_{\text{gene}}n_{\mathcal{V}}\mathcal{F}}{n_C})$ where n_C is the number of CPU cores. The space complexity is $O(n_{\mathcal{V}}Nd)$, where N, d are the number of qubits and circuit depth, respectively.

4 Method

4.1 Structure of GA

First, let us define some terminologies used in common genetic science and their counterpart in quantum circuits. These terminologies are given in Tab. 2 below.

In a GA scheme, each quantum circuit (individual gene) will be randomly generated from a pool gate with a fixed circuit depth, which consists of various types of quantum gates with one

Table 2. List of terminologies used in the common genetic science and theirs counterpart in quantum circuits.

Genetic science		Quantum circuit	
Name	Description	Name	Description
1 DNA/RNA	genetic material	quantum gate	unitary operator
2 individual	genetic unit	quantum circuit	a set of quantum gates
3 population	a group of genes	a set of quantum circuits	a set of quantum circuits
4 fitness	performance metric	cost function	performance metric

qubit, two-qubits, to one-parameter, and two-parameter. The more gates used, the more possible candidates. This increases the likelihood of finding a suitable candidate but at the same time expands the search space, making us spend more time. Furthermore, using basic gates such as Clifford set = {H, S, CX}⁴⁸ enables to implementation of candidates in a real quantum computer, two-qubits gates will be used restrictively. In general, our pool is {H, S, CX, R_i(.)} with $i \in \{x, y, z\}$.

The scheme will produce a set of quantum circuits and evaluate their fitness using a fitness function to identify the optimal quantum circuit. If the best fitness falls short of a predetermined threshold, an evolutionary process involving selection, crossover, and mutation will be implemented to generate a new circuit. This process will be repeated iteratively until the threshold is met or till the end number of generation, we then switch to VQA to optimize parameters Θ .

4.2 Selection-Crossover-Mutation

There are many types of selection, crossover, and mutation functions:

- Selection: Tournament, Proportional, Rank, Elitist,...
- Crossover: One-point, N-point, Uniform, Linear combination,...
- Mutation: Random deviation, Exchange, Shift, Bit flip, Inversion, Shuffle,...

In this work, we used Elitist Selection, One-point Crossover, and Bit Flip Mutation as the default option. We plan to investigate other combinations in future studies. After generating a set of quantum circuits \mathcal{V} , we evaluate them using cost functions like fidelity and retain only two best candidates as elitist circuits for the next generation. These selected candidates are paired for crossover to create new ones. Each pair of parents (p_1, p_2) is divided into four parts $\{p_{11}, p_{12}, p_{21}, p_{22}\}$ at one point, normally center point. Two new candidates (c_1, c_2) are formed by combining these parts: $c_1 = \{p_{11}, p_{22}\}$ and $c_2 = \{p_{21}, p_{12}\}$. In each generation, there is a small probability (1%) that any gate (bit) in a candidate will mutate and be replaced (flip) with a different gate from the pool.

4.3 Detailed experimental setting in the Results

All numerical findings are implemented in Python using Qiskit 0.45.1 with QASMSimulatorPy simulation to verify algorithm convergence. We benchmark 2 to 10 qubits on several computer

systems, including 24 nodes CPU Intel Xeon X5675 High-performance computer (HPC) at Vietnam Academy Science & Technology, Intel X299-GPU A6000 Workstation and AMD EPYC 7713P cluster @ Tohoku University, and Intel Core i9-10940X CPU at NAIST, Japan.

We mainly use gradient-based optimization with Adam optimizer (except for the VQE), where a set of θ is updated through

$$\theta^{k+1} = \theta^k - \alpha \frac{\hat{m}_k}{\sqrt{\hat{v}_k} + \epsilon}, \quad (14)$$

where $m_k = \beta_1 m_{k-1} + (1 - \beta_1) \nabla_{\theta} \mathcal{C}(\theta)$, $v_k = \beta_2 v_{k-1} + (1 - \beta_2) \nabla_{\theta}^2 \mathcal{C}(\theta)$, $\hat{m}_k = m_k / (1 - \beta_1^k)$, $\hat{v}_k = v_k / (1 - \beta_2^k)$, with the hyper-parameters are chosen as $\alpha = 0.2$, $\beta_1 = 0.8$, $\beta_2 = 0.999$ and $\epsilon = 10^{-8}$. The gradient $\partial_{\theta} \mathcal{C}(\theta)$ is given through the general parameter-shift rule⁴⁹.

Numerical benchmarking

For numerical benchmarking, we generated Haar random unitaries, using 20 for training and 10 for testing at each time. We ran GA-VQA on the training set with:

- $n_{\text{iter}} = 100$,
- threshold = 0.01,
- n_{gene} ranging from 10 to 40,
- $n_{\mathcal{V}} = [4, 8, 16, 32]$,
- Depth d from 2 to 39,

and get the best circuits for each setup. We use these best circuits to calculate the risk on the testing set. All results in Fig. 2 are for the testing set.

Thermal state preparation

Dense-purification method. We examine thermal state preparation using the dense-purification method across 2 to 10 qubits. Parameters include $n_{\text{iter}} = 100$, $d = 2N$, $n_{\mathcal{V}} = 8$, $n_{\text{gene}} = 16$. Note that n_{gene} does not significantly affect the runtime, as the program can stop anytime if the threshold is met. The threshold and optimizer remain consistent with the previous settings.

Conventional purification method. For the conventional purification method, we examine for $N = 2$ thermal state, which requires a 4-qubit circuit. Initially, we generate 100 target TFD states corresponding to equally-spaced $\beta \in [0, 10]$. We then run GA-VQA to find the best circuit structure for all those TFD states based on the weighted-sum cost function as we will explain below. Finally, we continue to run optimization using Adam optimizer for 100 iterations to find optimal parameters for each quantum state.

The circuit depth is 29 after transpiling. Other configurations include $n_{\text{iter}} = 100$, $n_{\mathcal{V}} = 16$, $n_{\text{gene}} = 20$. Furthermore, optimal parameters with $\beta < 1$ are harder to find than those with

$\beta > 1$. A simple average of cost values in the interval β from 0 to 10 is not sufficient for finding near-optimal ansatzes in the range β from 0 to 1. To address this, we use a weighted average cost function for different intervals. Specifically, we assign weights $w_1 = 2.2, w_2 = 1.6, w_3 = 0.9$ to three corresponding intervals $\beta \in [0, 4), \beta \in [4, 7),$ and $\beta \in [7, 10]$. The weighted-sum cost function is expressed as

$$\mathcal{F}_{\text{ws}} = \frac{w_1 * \mathcal{F}_{\beta \in [0,4)} + w_2 * \mathcal{F}_{\beta \in [4,7)} + w_3 * \mathcal{F}_{\beta \in [7,10]}}{w_1 + w_2 + w_3}, \quad (15)$$

where $\mathcal{F}_{\beta \in [i,j)}, 0 \leq i, j \leq 10$ is the average fidelity in the interval $[i, j)$.

Time-dependent dynamic simulation

GA-VQA method. For the GA-VQA method, our simulation follows these steps: (1) Create the initial state $|\psi_0\rangle = |11\dots00\rangle$ by applying X gates to $N/2$ qubits. (2) Create a set of 100 target unitaries $U(t_i)$ using Eq. (11) for $t_i \in [0, 10], i = \{1, 2, \dots, 100\}$. (3) We then run GA-VQA to find the best circuit structure for all those target unitaries. Once $V^*(\Theta^*)$ is determined, we measure the magnetization as follows. (i) Prepare $|\psi_0\rangle$ in a quantum circuit. (ii) Apply $V^*(\Theta^*)$ to get the final state $|\check{\psi}(t)\rangle = V^*(\Theta^*)|\psi_0\rangle$. (iii) Measure qubit j and get the probability

$$p_j(m) = \langle \check{\psi}(t) | \Pi_j | \check{\psi}(t) \rangle, \text{ for } m \in \{0, 1\}, \quad (16)$$

where $\Pi_j = I_1 \otimes \dots \otimes |m_j\rangle\langle m_j| \otimes \dots \otimes I_N$. Finally, the local magnetization (12) is given by

$$M_j(t) = p_j(0) - p_j(1). \quad (17)$$

We benchmark for 2-qubit case. The parameters used for this case include: $n_{\text{iter}} = 500, d = 4, n_V = 8, n_{\text{gene}} = 16$, and the local magnetization was taken for the second qubit. See Tab. 3 for a summary.

Trotterization method. To implement the trotterization, we break down the evolution $U(t_i)$ as follows

$$\begin{aligned} U(t_i) &= \exp \left[-i \int_{t_{i-1}}^{t_i} H(s) ds \right] \\ &= \exp \left\{ -i \frac{\delta t}{K} \lim_{K \rightarrow \infty} \left[H(t_{i-1}) + H(t_{i-1} + \frac{\delta t}{K}) + \dots + H(t_{i-1} + \frac{(K-1)\delta t}{K}) \right] \right\}, \end{aligned} \quad (18)$$

where $\delta t = t_i - t_{i-1} = 0.1$ is the interval, divided into K equal sub-intervals. Here, we set $K = 5$, making $\delta t/K = 0.02$ sufficiently small. Each $H(s)$ in the above expression consists of single and two-qubit gates, and we assume $H(s) = \sum_{j=1}^L H_j$. Using trotterization, we can break $H(s)$ into a sequence of quantum gates and implement it in quantum circuits. The trotterization expansions of the first order (Trotter1) and second order (Trotter2) are given by^{44,50}

$$e^{-iH(s)} = \lim_{r \rightarrow \infty} \left(e^{-i\frac{H_L}{r}} \dots e^{-i\frac{H_1}{r}} \right)^r \text{ for Trotter1, and} \quad (19)$$

$$e^{-iH(s)} = \lim_{r \rightarrow \infty} \left[\left(e^{-i\frac{H_L}{2r}} \dots e^{-i\frac{H_1}{2r}} \right) \left(e^{-i\frac{H_1}{2r}} \dots e^{-i\frac{H_L}{2r}} \right) \right]^r \text{ for Trotter2,} \quad (20)$$

where r is the Trotter number. In this work, we set $r = 100$.

AVQDS method. The AVQDS method, introduced in Ref.⁷, works as follows. Starting with the initial quantum state $|\psi_0\rangle$, the state evolves over time according to $|\psi(t)\rangle$ as

$$\frac{d|\psi(t)\rangle}{dt} = -iH(t)|\psi(t)\rangle. \quad (21)$$

To solve this, we use a variational quantum ansatz $|\psi(\boldsymbol{\theta}(t))\rangle$, where $\boldsymbol{\theta}(t)$ represents a set of time-dependent parameters. For example, at time $t = 0$, it gives $|\psi(\boldsymbol{\theta}(t = 0))\rangle = |\psi_0\rangle$. These parameters are trained to minimize the squared McLachlan distance⁵¹ \mathcal{L}^2

$$\mathcal{L}^2 = \left\| \sum_{\mu} \frac{d|\psi(\boldsymbol{\theta})\rangle}{d\theta_{\mu}} \frac{d\theta_{\mu}}{dt} + iH(t)|\psi(\boldsymbol{\theta})\rangle \right\|_F^2, \quad (22)$$

where $\|\cdot\|_F$ denotes the Frobenius norm, and we omit t in $\boldsymbol{\theta}(t)$ to simplify the notation.

In our numerical simulation, we first construct the Hamiltonian $H(t)$ as described in Eq. (10). We then employ the pseudo-Trotter ansatz⁷ $|\psi(\boldsymbol{\theta})\rangle = \prod_{\mu=1}^{N_{\boldsymbol{\theta}}} e^{-i\theta_{\mu} A_{\mu}} |\psi_0\rangle$, where $N_{\boldsymbol{\theta}}$ is the number of trainable time-dependent parameters, and A_{μ} are Hermitian operators from a set of Pauli operators. During the simulation for any time $0 < t_i < T$, the ansatz is adaptively updated until the squared McLachlan distance meets the threshold $\mathcal{L}_{\text{cut}}^2$. We set the threshold $\mathcal{L}_{\text{cut}}^2 = 10^{-3}$ for Fig. 4a, and $\mathcal{L}_{\text{cut}}^2 = 10^{-1}$ for Fig. 4b,c. In Fig. 4b,c, the AVQDS method is not trainable at $\mathcal{L}_{\text{cut}}^2 = 10^{-3}$, so we temporarily reduce its accuracy by training at $\mathcal{L}_{\text{cut}}^2 = 10^{-1}$. This is why the accuracy of this method is lower compared to the exact result and GA-VQA method.

Variational quantum eigensolver

For the variational quantum eigensolver^{46,52}, an upper bound of ground state energy E_o of a given Hamiltonian is bounded by

$$E_o \leq \frac{\langle \psi(\boldsymbol{\theta}) | H | \psi(\boldsymbol{\theta}) \rangle}{\langle \psi(\boldsymbol{\theta}) | \psi(\boldsymbol{\theta}) \rangle} \equiv \langle H \rangle, \quad (23)$$

which is found by optimizing the parameters of quantum state $|\psi\rangle \equiv V_l(\boldsymbol{\theta})|\mathbf{0}\rangle$. To simulate the GA-VQA scheme's application in VQE with a Hydrogen molecule, we run GA-VQA with the setup that can be seen in the VQE field at Tab. 3. In this case, the target of the GA-VQA is to find ansatzes with low depth but still gain the needed accuracy of ground state molecular energy. The Genetic Algorithm is leveraged to find the friendly NISQ ansatz while the optimizing part is left to VQE. This method iteratively converges to higher fidelity (the higher the fidelity, the more accurate the result) until the max generation or termination condition is satisfied.

Data availability

Data are available from the corresponding authors upon reasonable request.

Code availability

The code is available at <https://github.com/vutuanhai237/GA-QAS>.

Table 3. Experiment setting

Application	Benchmarking	TSP	TD-QDS	VQE
Cost function	$\mathcal{L}(5)$	$\mathcal{F}(9), \mathcal{F}_{ws}(15)$	$\mathcal{L}^2(22)$	$\mathcal{L}_{VQE}(13)$
Evaluated object	Haar random unitary	Thermal state	Heisenberg models	H_2 molecules
Optimizer	Adam	Adam	Adam	COBYLA
N	[2 – 5]	[2-10]	2	4
	$d = [2 - 39]$	$d = 2N$	$d = 4$	$d=[15,18,20,24,25]$
Hyper-parameter	$n_{\mathcal{V}} = [4, 8, 16, 32]$ $n_{\text{gene}} = [10, 20, 30, 40]$	$n_{\mathcal{V}} = 8$ $n_{\text{gene}} = 16$	$n_{\mathcal{V}} = 8$ $n_{\text{gene}} = 16$	$n_{\mathcal{V}} = 8$ $n_{\text{gene}} = 20$

Acknowledgment

V.T.H. thanks Dr. Luong Ngoc Hoang for advice on genetic algorithms. This research is funded by Vietnam National University Ho Chi Minh City (VNU-HCM) under grant number C2024-28-04, JSPS KAKENHI Grant Number 23K13025, Unitary Fund, and Tohoku University FRIS URO.

Author contributions statement

V.T.H. wrote the GA-QAS code and conducted the numerical simulation. N.T.V. and J.U. implemented the thermal state preparation. J.U. and L.B.H. carried out the time-dependent dynamics simulation. N.V.L. implemented the VQE demo. L.N.T proposed and supervised the VQE demo. L.B.H. proposed the theory of multi-target quantum compilation and supervised its application to thermal state preparation and time-dependent dynamics simulation. L.N.T and L.B.H. supervised the entire project. All authors discussed the results and contributed to writing the manuscript.

Competing interests

The author declares no competing interests.

References

1. Cerezo, M. *et al.* Variational quantum algorithms. *Nat. Rev. Phys.* **3**, 625–644, DOI: [10.1038/s42254-021-00348-9](https://doi.org/10.1038/s42254-021-00348-9) (2021).
2. Hai, V. T., Viet, N. T. & Ho, L. B. *jqo—opj*: A quantum object optimizer. *SoftwareX* **26**, 101726, DOI: <https://doi.org/10.1016/j.softx.2024.101726> (2024).
3. Kuzmin, V. V. & Silvi, P. Variational quantum state preparation via quantum data buses. *Quantum* **4**, 290, DOI: [10.22331/q-2020-07-06-290](https://doi.org/10.22331/q-2020-07-06-290) (2020).
4. Sagastizabal, R. *et al.* Variational preparation of finite-temperature states on a quantum computer. *npj Quantum Inf.* **7**, 130, DOI: [10.1038/s41534-021-00468-1](https://doi.org/10.1038/s41534-021-00468-1) (2021).

5. Castro, J. C. Z. *et al.* Variational quantum state preparation for quantum-enhanced metrology in noisy systems (2024). [2406.01859](#).
6. Hai, V. T., Viet, N. T. & Ho, L. B. Variational preparation of entangled states on quantum computers. *arXiv preprint arXiv:2306.17422* (2023).
7. Yao, Y.-X. *et al.* Adaptive variational quantum dynamics simulations. *PRX Quantum* **2**, 030307, DOI: [10.1103/PRXQuantum.2.030307](#) (2021).
8. Luo, J., Lin, K. & Gao, X. Variational quantum simulation of lindblad dynamics via quantum state diffusion. *The J. Phys. Chem. Lett.* **15**, 3516–3522, DOI: [10.1021/acs.jpcllett.4c00576](#) (2024).
9. Linteau, D., Barison, S., Lindner, N. H. & Carleo, G. Adaptive projected variational quantum dynamics. *Phys. Rev. Res.* **6**, 023130, DOI: [10.1103/PhysRevResearch.6.023130](#) (2024).
10. Koczor, B., Endo, S., Jones, T., Matsuzaki, Y. & Benjamin, S. C. Variational-state quantum metrology. *New J. Phys.* **22**, 083038, DOI: [10.1088/1367-2630/ab965e](#) (2020).
11. Ma, Z. *et al.* Adaptive circuit learning for quantum metrology. In *2021 IEEE International Conference on Quantum Computing and Engineering (QCE)*, 419–430, DOI: [10.1109/QCE52317.2021.00063](#) (2021).
12. Meyer, J. J., Borregaard, J. & Eisert, J. A variational toolbox for quantum multi-parameter estimation. *npj Quantum Inf.* **7**, 89, DOI: [10.1038/s41534-021-00425-y](#) (2021).
13. Le, T. K., Nguyen, H. Q. & Ho, L. B. Variational quantum metrology for multiparameter estimation under dephasing noise. *Sci. Reports* **13**, 17775, DOI: [10.1038/s41598-023-44786-0](#) (2023).
14. Cimini, V. *et al.* Variational quantum algorithm for experimental photonic multiparameter estimation. *npj Quantum Inf.* **10**, 26, DOI: [10.1038/s41534-024-00821-0](#) (2024).
15. Heya, K., Suzuki, Y., Nakamura, Y. & Fujii, K. Variational quantum gate optimization (2018). [1810.12745](#).
16. Khatri, S. *et al.* Quantum-assisted quantum compiling. *Quantum* **3**, 140, DOI: [10.22331/q-2019-05-13-140](#) (2019).
17. Volkoff, T., Holmes, Z. & Sornborger, A. Universal compiling and (no-)free-lunch theorems for continuous-variable quantum learning. *PRX Quantum* **2**, 040327, DOI: [10.1103/PRXQuantum.2.040327](#) (2021).
18. Hai, V. T. & Ho, L. B. Universal compilation for quantum state tomography. *Sci. Reports* **13**, 3750, DOI: [10.1038/s41598-023-30983-4](#) (2023).
19. Du, Y., Huang, T., You, S., Hsieh, M.-H. & Tao, D. Quantum circuit architecture search for variational quantum algorithms. *npj Quantum Inf.* **8**, 62, DOI: [10.1038/s41534-022-00570-y](#) (2022).

20. Zhang, S.-X., Hsieh, C.-Y., Zhang, S. & Yao, H. Neural predictor based quantum architecture search. *Mach. Learn. Sci. Technol.* **2**, 045027, DOI: [10.1088/2632-2153/ac28dd](https://doi.org/10.1088/2632-2153/ac28dd) (2021).

21. Li, L., Fan, M., Coram, M., Riley, P. & Leichenauer, S. Quantum optimization with a novel gibbs objective function and ansatz architecture search. *Phys. Rev. Res.* **2**, 023074, DOI: [10.1103/PhysRevResearch.2.023074](https://doi.org/10.1103/PhysRevResearch.2.023074) (2020).

22. He, Z., Chen, C., Li, L., Zheng, S. & Situ, H. Quantum architecture search with meta-learning. *Adv. Quantum Technol.* **5**, 2100134, DOI: <https://doi.org/10.1002/qute.202100134> (2022). <https://onlinelibrary.wiley.com/doi/pdf/10.1002/qute.202100134>.

23. Grimsley, H. R., Economou, S. E., Barnes, E. & Mayhall, N. J. An adaptive variational algorithm for exact molecular simulations on a quantum computer. *Nat. Commun.* **10**, 3007, DOI: [10.1038/s41467-019-10988-2](https://doi.org/10.1038/s41467-019-10988-2) (2019).

24. Rubinstein, B. Evolving quantum circuits using genetic programming. In *Proceedings of the 2001 Congress on Evolutionary Computation (IEEE Cat. No.01TH8546)*, vol. 1, 144–151 vol. 1, DOI: [10.1109/CEC.2001.934383](https://doi.org/10.1109/CEC.2001.934383) (2001).

25. Lambora, A., Gupta, K. & Chopra, K. Genetic algorithm- a literature review. In *2019 International Conference on Machine Learning, Big Data, Cloud and Parallel Computing (COMITCon)*, 380–384, DOI: [10.1109/COMITCon.2019.8862255](https://doi.org/10.1109/COMITCon.2019.8862255) (2019).

26. Katoch, S., Chauhan, S. S. & Kumar, V. A review on genetic algorithm: past, present, and future. *Multimed. Tools Appl.* **80**, 8091–8126, DOI: [10.1007/s11042-020-10139-6](https://doi.org/10.1007/s11042-020-10139-6) (2021).

27. Tandeitnik, D. & Guerreiro, T. Evolving quantum circuits. *Quantum Inf. Process.* **23**, DOI: [10.1007/s11128-024-04317-w](https://doi.org/10.1007/s11128-024-04317-w) (2024).

28. Ostaszewski, M., Grant, E. & Benedetti, M. Structure optimization for parameterized quantum circuits. *Quantum* **5**, 391, DOI: [10.22331/q-2021-01-28-391](https://doi.org/10.22331/q-2021-01-28-391) (2021).

29. Creevey, F. M., Hill, C. D. & Hollenberg, L. C. L. Gasp: a genetic algorithm for state preparation on quantum computers. *Sci. Reports* **13**, 11956, DOI: [10.1038/s41598-023-37767-w](https://doi.org/10.1038/s41598-023-37767-w) (2023).

30. Caro, M. C. *et al.* Out-of-distribution generalization for learning quantum dynamics. *Nat. Commun.* **14**, 3751, DOI: [10.1038/s41467-023-39381-w](https://doi.org/10.1038/s41467-023-39381-w) (2023).

31. Ezzell, N. *et al.* Quantum mixed state compiling. *Quantum Sci. Technol.* **8**, 035001 (2023).

32. Leamer, J. M., Zhang, W., Saripalli, R. K., Glasser, R. T. & Bondar, D. I. Simulation of quantum gibbs states using epsilon-near-zero materials and classical light. In *Conference on Lasers and Electro-Optics*, JTU3A.72 (Optica Publishing Group, 2021).

33. Amin, M. H., Andriyash, E., Rolfe, J., Kulchytskyy, B. & Melko, R. Quantum boltzmann machine. *Phys. Rev. X* **8**, 021050, DOI: [10.1103/PhysRevX.8.021050](https://doi.org/10.1103/PhysRevX.8.021050) (2018).

34. Coopmans, L., Kikuchi, Y. & Benedetti, M. Predicting gibbs-state expectation values with pure thermal shadows. *PRX Quantum* **4**, 010305, DOI: [10.1103/PRXQuantum.4.010305](https://doi.org/10.1103/PRXQuantum.4.010305) (2023).

35. Lewin, M., Nam, P. T. & Rougerie, N. Classical field theory limit of many-body quantum gibbs states in 2d and 3d. *Invent. mathematicae* **224**, 315–444, DOI: [10.1007/s00222-020-01010-4](https://doi.org/10.1007/s00222-020-01010-4) (2021).

36. Israel, W. Thermo-field dynamics of black holes. *Phys. Lett. A* **57**, 107–110, DOI: [https://doi.org/10.1016/0375-9601\(76\)90178-X](https://doi.org/10.1016/0375-9601(76)90178-X) (1976).

37. Gao, P., Jafferis, D. L. & Wall, A. C. Traversable wormholes via a double trace deformation. *J. High Energy Phys.* **2017**, 151, DOI: [10.1007/JHEP12\(2017\)151](https://doi.org/10.1007/JHEP12(2017)151) (2017).

38. Ho, W. W. & Hsieh, T. H. Efficient variational simulation of non-trivial quantum states. *SciPost Phys.* **6**, 029, DOI: [10.21468/SciPostPhys.6.3.029](https://doi.org/10.21468/SciPostPhys.6.3.029) (2019).

39. Wu, J. & Hsieh, T. H. Variational thermal quantum simulation via thermofield double states. *Phys. Rev. Lett.* **123**, 220502, DOI: [10.1103/PhysRevLett.123.220502](https://doi.org/10.1103/PhysRevLett.123.220502) (2019).

40. Zhu, D. *et al.* Generation of thermofield double states and critical ground states with a quantum computer. *Proc. Natl. Acad. Sci.* **117**, 25402–25406, DOI: [10.1073/pnas.2006337117](https://doi.org/10.1073/pnas.2006337117) (2020).

41. Wang, Y., Li, G. & Wang, X. Variational quantum gibbs state preparation with a truncated taylor series. *Phys. Rev. Appl.* **16**, 054035, DOI: [10.1103/PhysRevApplied.16.054035](https://doi.org/10.1103/PhysRevApplied.16.054035) (2021).

42. Premaratne, S. P. & Matsuura, A. Y. Engineering a cost function for real-world implementation of a variational quantum algorithm. In *2020 IEEE International Conference on Quantum Computing and Engineering (QCE)*, DOI: [10.1109/qce49297.2020.00042](https://doi.org/10.1109/qce49297.2020.00042) (IEEE, 2020).

43. Ikeda, T. N., Abrar, A., Chuang, I. L. & Sugiura, S. Minimum Trotterization Formulas for a Time-Dependent Hamiltonian. *Quantum* **7**, 1168, DOI: [10.22331/q-2023-11-06-1168](https://doi.org/10.22331/q-2023-11-06-1168) (2023).

44. Ikeda, T. N., Kono, H. & Fujii, K. Trotter24: A precision-guaranteed adaptive stepsize trotterization for hamiltonian simulations (2023). [2307.05406](https://doi.org/10.4236/qe.20230705406).

45. Zhao, H., Bukov, M., Heyl, M. & Moessner, R. Adaptive trotterization for time-dependent hamiltonian quantum dynamics using instantaneous conservation laws (2023). [2307.10327](https://doi.org/10.4236/qe.20230705327).

46. Peruzzo, A. *et al.* A variational eigenvalue solver on a photonic quantum processor. *Nat. Commun.* **5**, 4213, DOI: [10.1038/ncomms5213](https://doi.org/10.1038/ncomms5213) (2014).

47. Romero, J. *et al.* Strategies for quantum computing molecular energies using the unitary coupled cluster ansatz. *Quantum Sci. Technol.* **4**, 014008, DOI: [10.1088/2058-9565/aad3e4](https://doi.org/10.1088/2058-9565/aad3e4) (2018).

48. Gottesman, D. Theory of fault-tolerant quantum computation. *Phys. Rev. A* **57**, 127–137, DOI: [10.1103/PhysRevA.57.127](https://doi.org/10.1103/PhysRevA.57.127) (1998).

49. Hai, V. T. & Ho, L. B. *Lagrange Interpolation Approach for General Parameter-Shift Rule*, 1–17 (Springer International Publishing, Cham, 2024).

50. Layden, D. First-order trotter error from a second-order perspective. *Phys. Rev. Lett.* **128**, 210501, DOI: [10.1103/PhysRevLett.128.210501](https://doi.org/10.1103/PhysRevLett.128.210501) (2022).
51. McLachlan, A. A variational solution of the time-dependent schrodinger equation. *Mol. Phys.* **8**, 39–44, DOI: [10.1080/00268976400100041](https://doi.org/10.1080/00268976400100041) (1964). <https://doi.org/10.1080/00268976400100041>.
52. Tilly, J. *et al.* The variational quantum eigensolver: A review of methods and best practices. *Phys. Reports* **986**, 1–128, DOI: <https://doi.org/10.1016/j.physrep.2022.08.003> (2022). The Variational Quantum Eigensolver: a review of methods and best practices.